Supplement of Hydrol. Earth Syst. Sci., 25, 983–1007, 2021
https://doi.org/10.5194/hess-25-983-2021-supplement

Hydrology and Earth System Sciences
Open Access
EGU

Supplement of

Sigmoidal water retention function with improved behaviour in dry and wet soils

Gerrit Huibert de Rooij et al.

Correspondence to: Gerrit Huibert de Rooij (gerrit.derooij@ufz.de) and Raneem Madi (rmadi@gfi-dresden.de)

Generating weather records for monsoon, semi–arid, and temperate climates

The weather generator TEmpotRain (de Rooij, 2018) was used to generate 1000–year records of daily rainfall, temperature (daily mean, minimum, and maximum), solar radiation, and daily potential evapotranspiration (ET_{pot}). The latter was calculated from the solar radiation and the temperatures according to de Rooij's (2018) version of the modified Hargreaves equation (Droogers and Allen, 2002). Droogers and Allen (2002) showed that their modification (which takes into account the monthly rainfall sums) improves the results, especially for drier climates. De Rooij (2018) used the rainfall sum in a 30–day moving time window instead of monthly sums. He also implemented Evett's (2000, p. A150) temperature correction that accounts for the energy that is used to warm up the soil water and therefore is not available to turn liquid water into vapor.

The weather statistics to characterize the three climates (Table 1 in the main text) are based on the 1000–year records. The numerical simulations of soil water flow were carried out with the first 16 years of these records.

The weather generator (de Rooij, 2018) requires input parameters that define the weather that needs to be generated. The rainfall parameters for the monsoon climate are given in Table S1, those for the semi–arid climate in Table S2, and those for the temperate climate in Table S3. The parameters governing the temperature and ET_{pot} for all climates are listed in Table S4. De Rooij (2018) explains the meaning and purpose of the various parameters. Tables S1–S3 follow the notation of Table 1 of de Rooij (2018). In cases where the symbols used there are used for other variable in this paper they have the subscript 'wg' in this supplement to indicate they relate to the weather generator. Table S4 follows the notation of Table 5 in de Rooij (2018).

Table S1. The parameters governing rainfall of the monsoon climate.

Period	Start time (d)	λ_{wg} (d^{-1})	p	δ ($\mathrm{d\ mm}^{-1}$)	α_{wg}	ν (d)	κ	φ	ε (d^{-1})
1	0.0	0.300	1.50	0.0124	1.50	0.0156	0.750	0.250	6.91
2	60.0	0.578	1.50	0.0357	1.80	0.188	1.25	0.625	4.61
3	152.0	0.575	1.60	0.0320	2.00	0.100	0.600	0.300	9.21
4	274.0	0.667	1.20	0.0522	1.20	0.100	2.00	0.333	3.84
5	335.0	0.300	1.50	0.0124	1.50	0.0156	0.750	0.250	6.91

Table S2. The parameters governing rainfall of the semi–arid climate.

Period	Start time (d)	λ_{wg} (d^{-1})	p	δ ($\mathrm{d\ mm}^{-1}$)	α_{wg}	ν (d)	κ	φ	ε (d^{-1})
1	0.0	0.060	1.20	0.0233	1.50	0.0313	1.50	0.500	6.14
2	106.0	0.350	1.80	0.0356	4.00	0.167	2.00	0.500	6.14
3	213.0	0.567	1.50	0.0564	2.00	0.167	2.00	0.500	4.61
4	281.0	0.060	1.20	0.0233	1.50	0.0313	1.50	0.500	6.14

The rainfall data for the temperate climate were taken from the literature (Pham et al., 2013). The other weather parameters were fitted by trial and error to (sometimes scant) weather data available from various on–line sources for the regions near the cities of Colombo in Sri Lanka (monsoon climate), Tamale in Ghana (semi–arid climate), and Ukkel in Belgium (temperate climate). Note that the first and last lines in Tables S1 and S2 are identical. This indicates that one of the periods for which rainfall generator parameters needed to be specified started late in the year and continued into the next year.

Table S3. The parameters governing rainfall of the temperate climate (Pham et al., 2013).

Period	λ_{wg} (d^{-1})	p	δ (d mm^{-1})	α_{wg}	ν (d)	κ	φ	ε (d^{-1})
Jan	0.768	2.304	0.0680	3.000	0.0320	0.200	0.046	1.52E−14
Feb	0.672	2.663	0.0777	3.000	0.0316	0.193	0.044	2.22E−14
Mar	0.648	1.463	0.0413	3.000	0.0268	0.223	0.044	1.38E−14
Apr	0.648	2.525	0.0525	3.000	0.0196	0.157	0.030	6.00E−14
May	0.576	0.696	0.0290	3.788	0.0274	0.167	0.035	4.08E−12
Jun	0.552	0.654	0.0273	5.292	0.0458	0.162	0.035	6.05
Jul	0.576	0.429	0.0179	5.893	0.0448	0.149	0.030	11.1
Aug	0.672	0.716	0.0298	3.000	0.0151	0.217	0.046	2.93E−13
Sep	0.600	0.923	0.0385	3.000	0.0179	0.176	0.035	1.02E−13
Oct	0.552	1.523	0.0635	3.000	0.0343	0.166	0.038	3.82E−14
Nov	0.696	1.519	0.0633	3.000	0.0343	0.190	0.040	1.72E−13
Dec	0.720	1.936	0.0807	3.000	0.0373	0.180	0.043	2.25E−14

Table S4. Parameters for the temperature, cloudiness, and evapotranspiration. The parameters are explained in de Rooij (2018, Table 5).

Parameter	Monsoon climate	Semi–arid climate	Temperate climate
$\bar{T}_a$ (°C)	27.2	27.9	10.6
σ_T (°C)	2.0	4.0	0.0
A_c (°C)	1.1	2.02	6.0
A_o (°C)	0.7	1.0	3.0
σ_a (°C)	0.20	0.20	2.5
ψ (d)	−48.7	29.7	−122
ϕ	0.60	0.6	0.6
σ_m (°C)	0.20	0.20	2.0
μ_f	1.89	1.76	1.19
$\sigma_{f,c}$	0.16	0.25	0.29
$\sigma_{f,o}$	0.10	0.074	0.15
P_l (mm)	2.0	2.0	2.0
P_h (mm)	50.0	60.0	20.0
f_1	0.10	0.01	0.25
f_2	0.60	0.20	0.95
f_3	0.95	0.30	0.35
Latitude (rad)	0.1190	0.1658	0.8866

Model simulations to test the performance of different parameterizations of the soil water retention curve

The simulations assumed a grass cover of 10 cm height in all cases. We realize this is not realistic for the semi–arid climate but kept the soil cover the same for all climates to facilitate the comparison between soils and climates. Roots were uniformly distributed in a 50 cm root zone, roughly representative for several grasses (e.g., Brown et al., 2010). For simplicity, interception was neglected. Surface ponding was allowed up to a depth of 1.0 cm. The soil was uniform over the simulation depth of 2.00 m, with a unit–gradient lower boundary condition. Heat flow and vapor flow were not considered.

The three soils used in the simulations and the values of their parameters are given in Table 2 of the main text. The acronyms for the parameterizations used here, as well as their equations, are also given in the main text.

The initial time step of the numerical solution was 0.001 d. The parameters governing the incremental increase and decrease of the time step were set to the default values, while the parameters of the convergence criteria were set to the values recommended in the manual (Šimůnek et al., 2013, p. 189). The nodal distance was smallest near the surface (4 mm), and gradually increased to reach 19 mm in the region below the root zone. In the lower 5 cm of the profile, the nodal distance decreased gradually to 11 mm at the bottom. The total number of nodes was 151. The simulated period was 16 years. For the analysis that follows, only the final six years were considered in order to minimize the effect of the initial conditions.

Initially, the soil was at hydrostatic equilibrium with the groundwater level at 2.00 m depth. The upper boundary condition gave the daily precipitation rate during rainy days, converted to a sinusoidal function internally by Hydrus–1D. During dry days, the matric potential at the soil surface was not allowed to fall below -10^7 cm. Daily values of potential evapotranspiration (ET_{pot}) were also provided on input. The albedo of the grass was set to 0.23 for all soils and climates, in line with reported values (e.g., Davies, 1967; Grant et al., 2000).

The partitioning of daily ET_{pot} as generated by TEmpotRain into daily potential evaporation (E_{pot}) and transpiration (T_{pot}) was done internally by Hydrus–1D. The leaf area index (LAI) was set to 2.4 for grass of the selected height (Šimůnek et al., 2013, p. 229). From that the model calculated the soil cover fraction (SCF) as (Šimůnek et al., 2013, p. 229)

$$\text{SCF} = 1 - \text{e}^{-0.463\ \text{LAI}} = 0.671 \tag{S1}$$

The partitioning of ET_{pot} was then straightforward (Šimůnek et al., 2013, p. 38):

$$T_{\text{pot}} = ET_{\text{pot}}\text{SCF} = 0.671 ET_{\text{pot}} \tag{S2}$$

$$E_{\text{pot}} = ET_{\text{pot}} - T_{\text{pot}} = 0.329 ET_{\text{pot}} \tag{S3}$$

These daily values were internally converted to low night–time values and higher, sinusoidal daytime values by the model (Šimůnek et al., 2013, p. 38).

Simulation results

The monsoon climate represented a region close to the equator (6°49′ N lat), and the annual variation in ET_{pot} is therefore limited (Top panels of Fig. S1–S3). The seasonality of the rainfall led to significant drops in E_{act} and T_{act} calculated with RIA during the dry seasons. These drops were more pronounced for clay (Fig. S1) and loamy sand (Fig. S3) than for silt loam (Fig. S2).

The values of E_{act} and T_{act} did not differ much between parameterizations for either silt loam (Fig. 4) or loamy sand (Fig. S3), and they ranged in bands whose bounds were dominated more by rainfall than by season. The flow across the lower boundary (deep drainage) was also dominated by rainfall for all three textures (Fig. S1–S3). For silt loam (Fig. S2) deep drainage for VGA was markedly less smooth than for VGN, with RIA in between. The same behavior emerged for loamy sand (Fig. S3), but with an overall reduced damping of the response to the rainfall signal compared to silt loam.

The semi–arid location was a little farther away from the equator (9°30′ N lat) than the monsoon location, and had a wet and a dry season. Potential evapotranspiration was consistently high (Fig. S4–S6, top panels), but the separation between E_{act} and T_{act} for all soils with the RIA parameterization (Fig. S4–S6, top panels) was less pronounced than that for the monsoon climate.

For clay, RIA gave near–zero values for E_{act} and T_{act} during the dry seasons (Fig. S4) with short bursts of evapotranspiration after an occasional storm. Deep drainage in clay occurred infrequently, and only during the rainy season (Fig. S4).

For silt loam, E_{act} of all three parameterizations dropped sharply at the end of the rainy season, and for some years even during dry periods within the rainy season (Fig. S5). Unsurprisingly, this effect was stronger for loamy sand (Fig. S6). Loamy sand's separation between E_{act} and T_{act} was somewhat more pronounced than that for silt loam. Silt loam allowed transpiration to occur for longer and at a higher rate during the dry season than loamy sand. For both soils, RIA tended to allow higher transpiration rates during the dry season than VGA and VGN.

Deep drainage was rare in the semi–arid climate, and varied strongly between the years, depending on the annual rainfall. For both silt loam and loamy sand, VGA generated deep drainage more often and at a higher rate that VGN, with RIA in between but much closer to VGN than to VGA (Fig. S4–S6).

The location with the moderate climate was far away from the equator (50°48′ N lat), resulting in a strong seasonal trend in ET_{pot} (Fig. S7–S9, top panels). There were wetter and drier periods, but no real dry season. For all soils, both E_{act} and T_{act} dropped in winter in response the very low E_{pot} in that season (Fig. S7–S9). In clay, the rainfall deficit in summer led to a drop in T_{act} in late spring/early summer while E_{act} was affected much less.

The silt loam had a high water holding capacity, and the reduction in T_{act} in the summer was less severe than for clay (Fig. S8). Still, there were many days with strongly reduced evapotranspiration rates in the second and fourth year. The dry summer periods were punctuated by brief intervals of increased evapotranspiration in response to rainfall.

In loamy sand, the decline of T_{act} in particular was rapid and deep in late spring or early summer due to the rainfall deficit that caused the root zone to dry out (Fig. S9). The limited water holding capacity of this relatively coarse–textured soil made these effects much more pronounced compared to the other soils: every year had a large number of days with very low evapotranspiration. VGA's evapotranspiration was more sensitive to the rainfall signal than that of VGA or RIA.

The rainfall excess in winter could sustain a downward flux at 2 m depth almost year–round for the RIA parameterization of clay (Fig. S7). For the silt loam (Fig. S8), both VGN and RIA had year–round deep drainage, while VGA showed much higher peaks during wet periods that arrived well before those of VGA and RIA but dropped off much faster and reached negligible values for some period of time every year. For the loamy sand (Fig. S9) VGA still had the highest peak of deep drainage, but the difference in the levels and arrival times of the peaks was smaller than for silt loam. Deep drainage became negligible for roughly half of the time for VGA and for shorter periods for VGN and RIA.

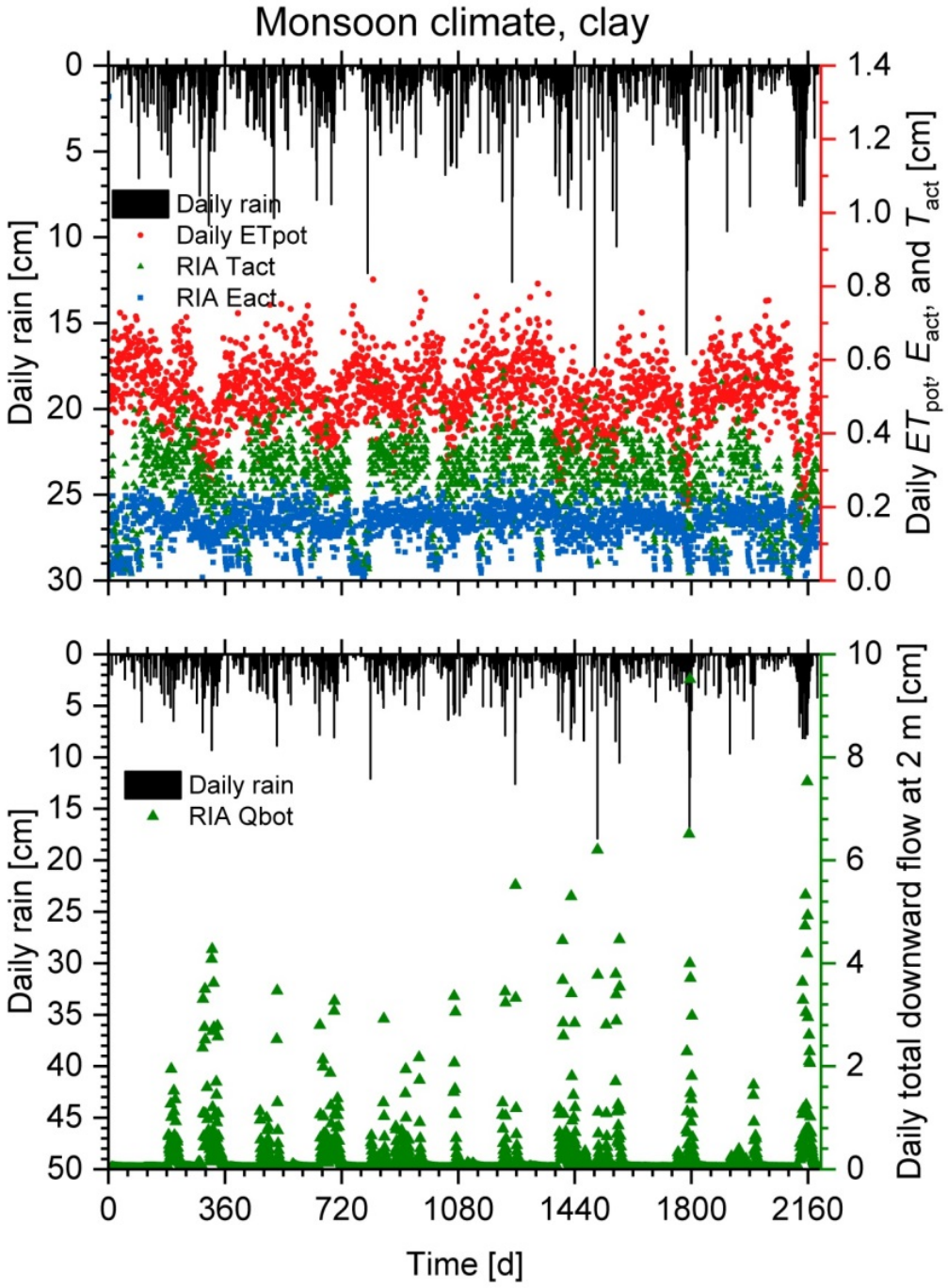

Figure S1. Generated rainfall and potential evapotranspiration (ET_{pot}) for a monsoon climate, and the simulated actual transpiration (E_{act}) and evaporation (T_{act}) (top panel), as well as the daily downward flow at 2 m depth (bottom panel) for a clay soil. The graphs cover a six–year period starting at January 1st. The second and sixth year are leap years. Simulations results are shown for the RIA parameterization only because the other parameterizations did not run successfully. The parameterizations are explained in Fig. 1 and the main text.

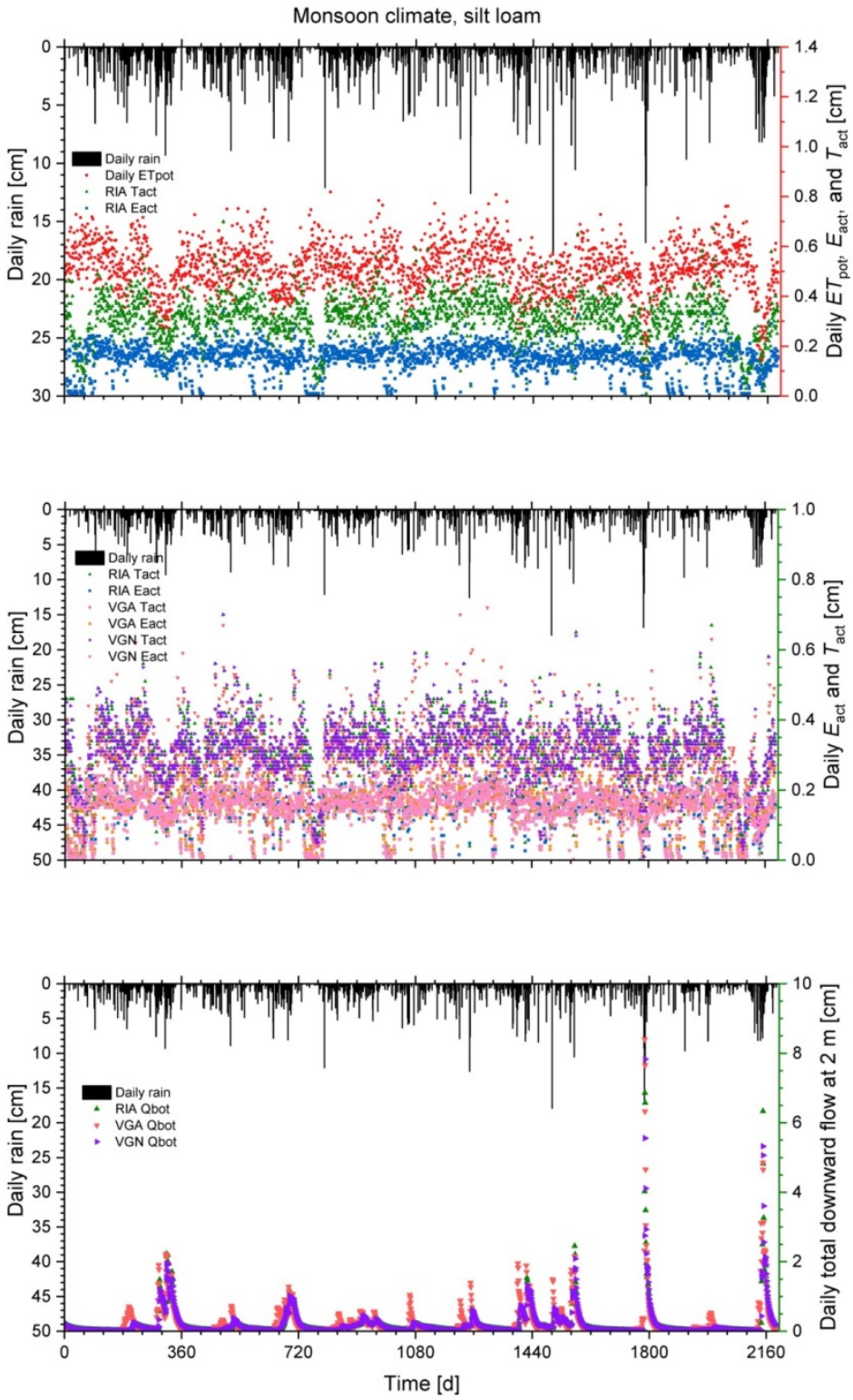

Figure S2. The weather data are those of Fig. S1, but the soil is a silt loam. The top panel shows the weather data and actual transpiration (E_{act}) and evaporation (T_{act}) according to the RIA parameterization. The middle panel shows E_{act} and T_{act} for the VGN, VGA, and RIA parameterizations for comparison. The bottom panel has the downward fluxes at 2 m depth for all three parameterizations.

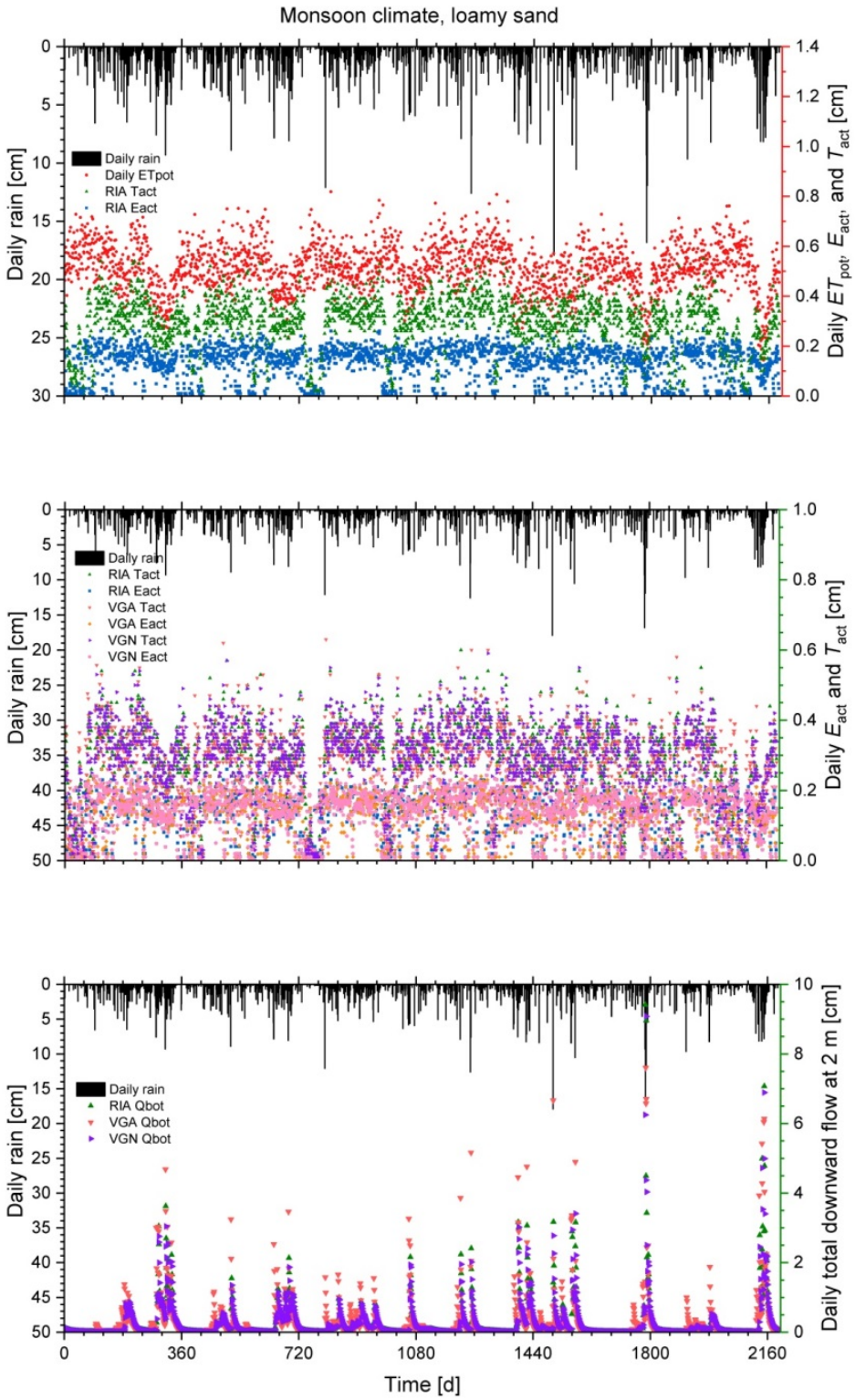

Figure S3. The weather data are those of Fig. S1, but the soil is a loamy sand. The top panel shows the weather data and actual transpiration (E_{act}) and evaporation (T_{act}) according to the RIA parameterization. The middle panel shows E_{act} and T_{act} for the VGN, VGA, and RIA parameterizations for comparison. The bottom panel has the downward fluxes at 2 m depth for all three parameterizations.

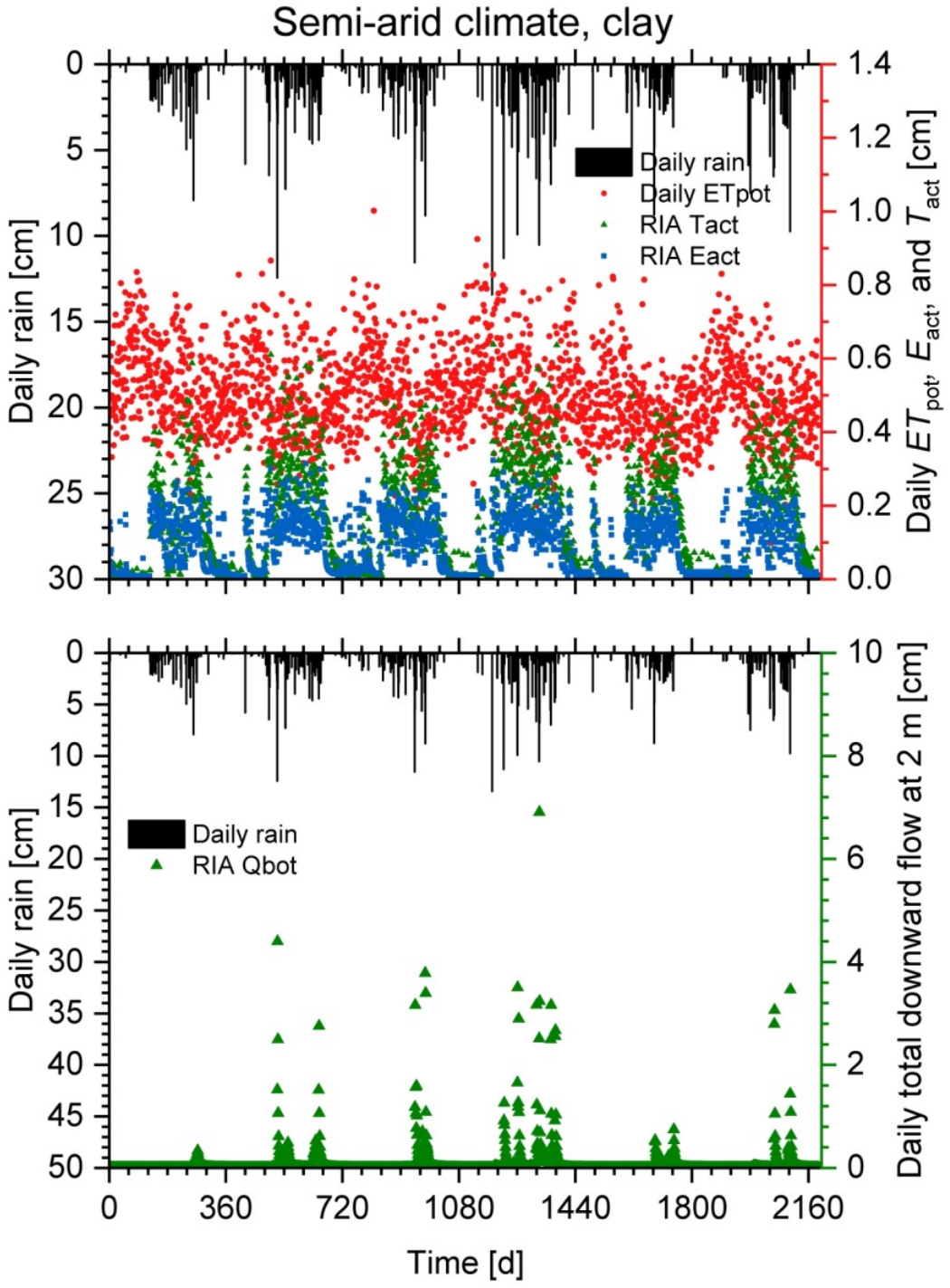

Figure S4. Like Fig. S1, but for a semi–arid climate.

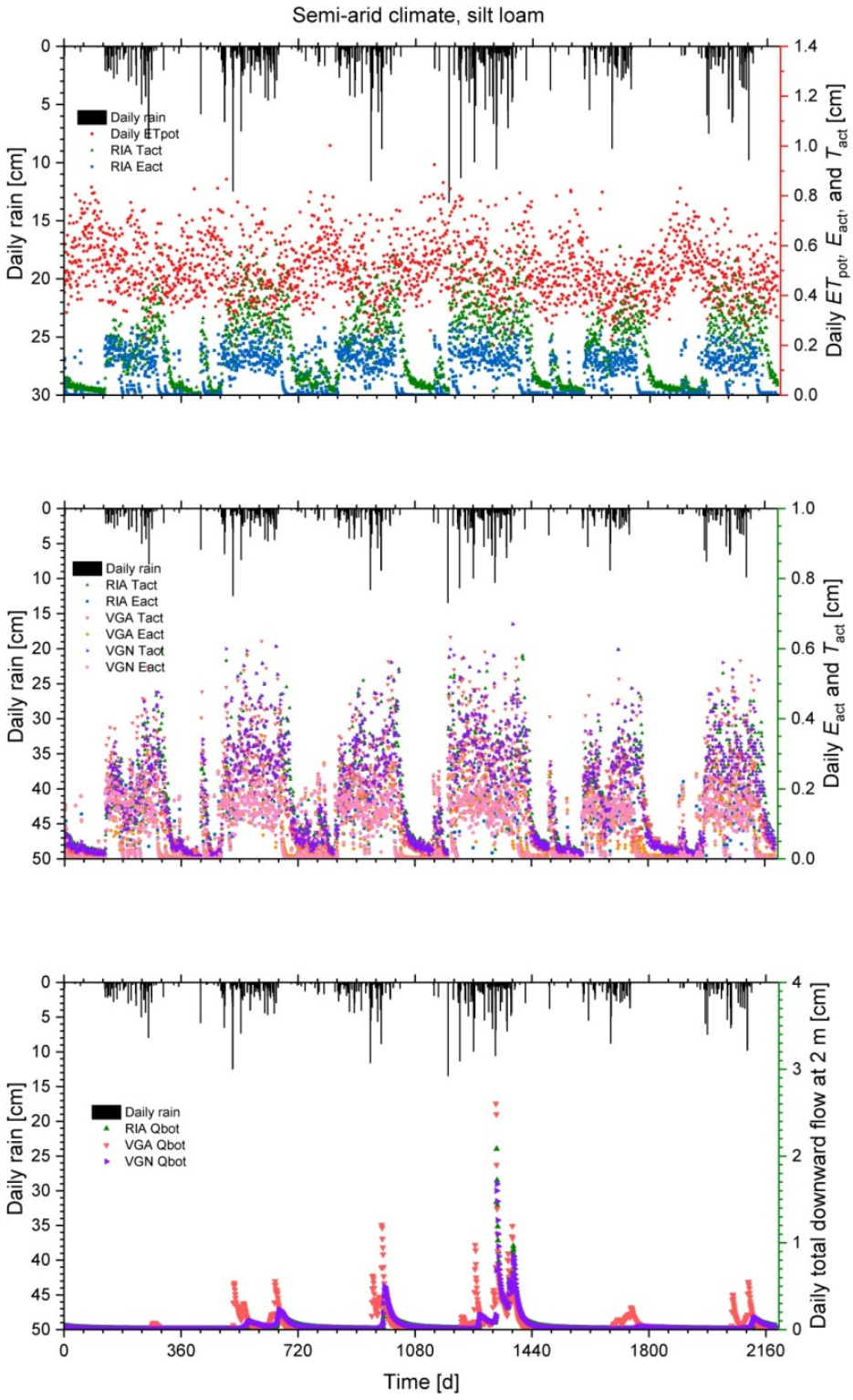

Figure S5. Like Fig. S2, but for a semi–arid climate.

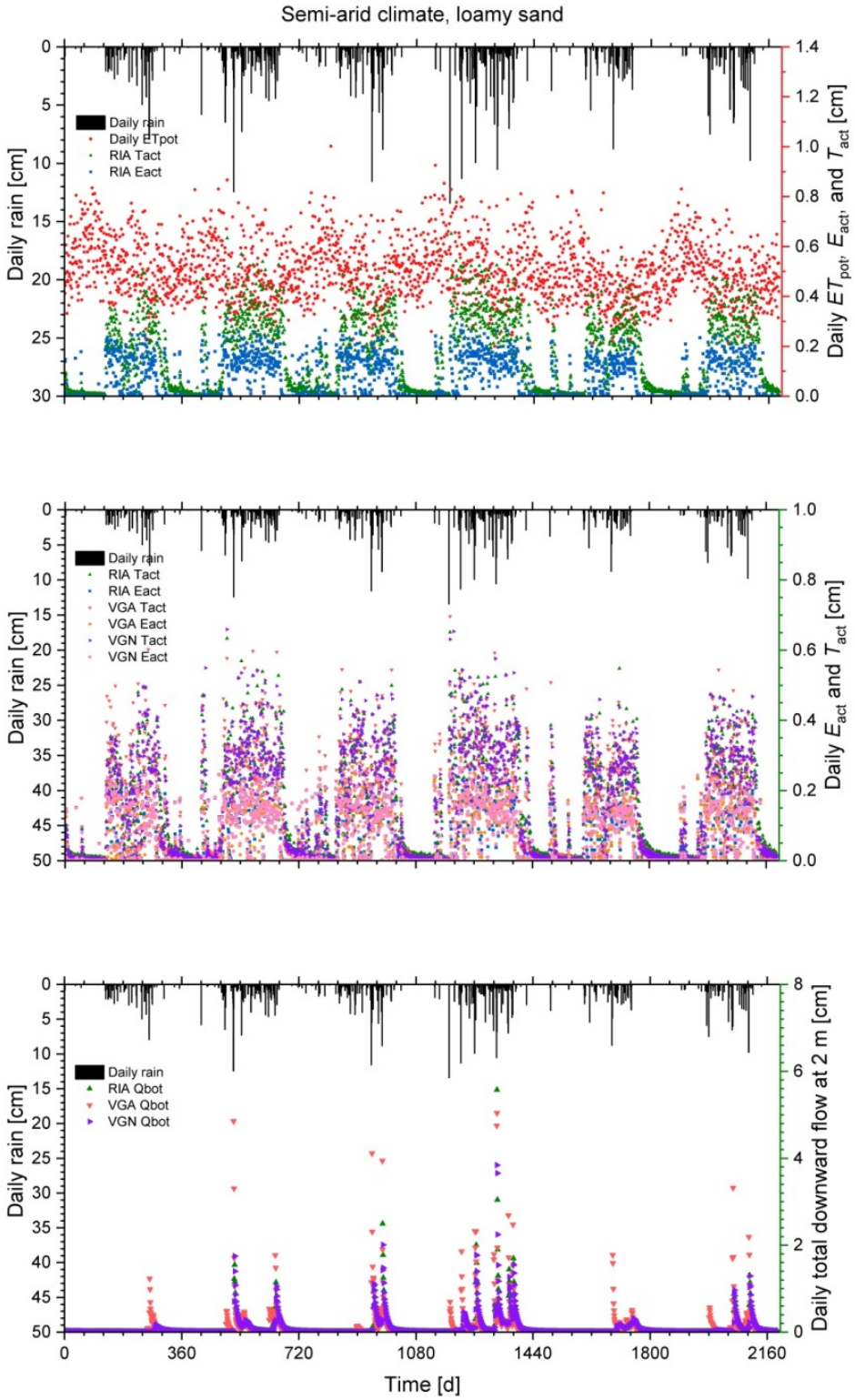

Figure S6. Like Fig. S3, but for a semi–arid climate.

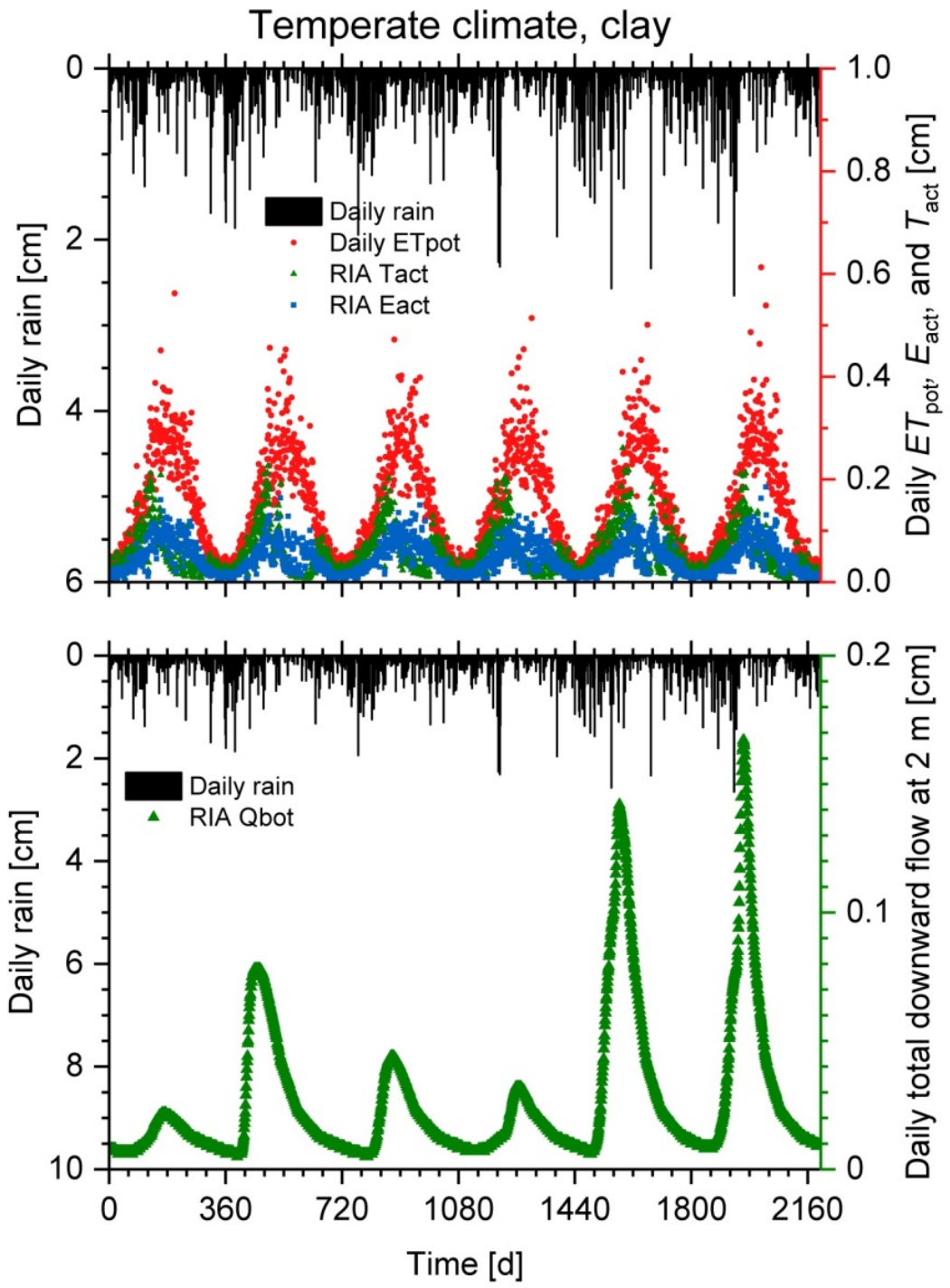

Figure S7. Like Fig. S1, but for a temperate climate.

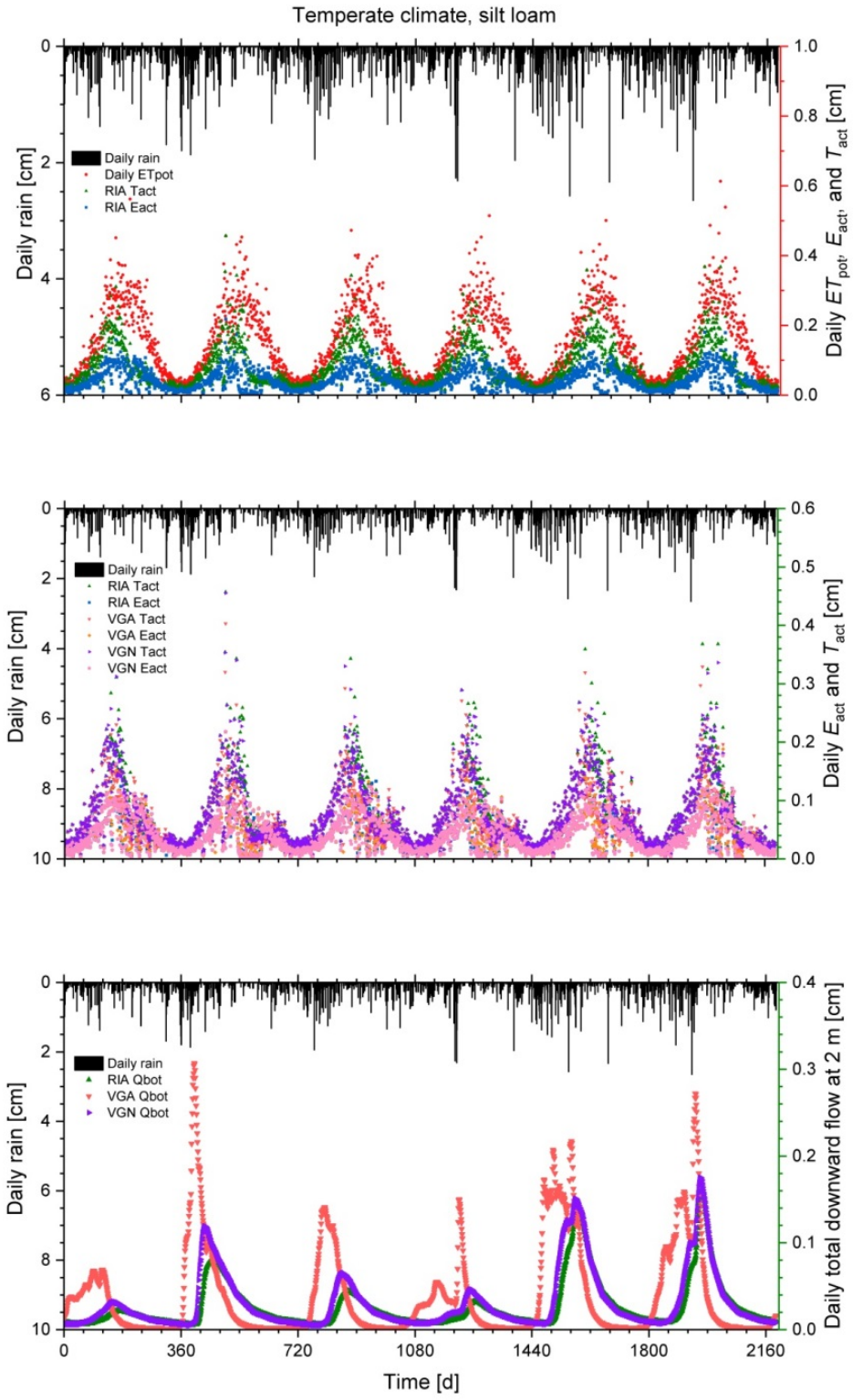

Figure S8. Like Fig. S2, but for a temperate climate.

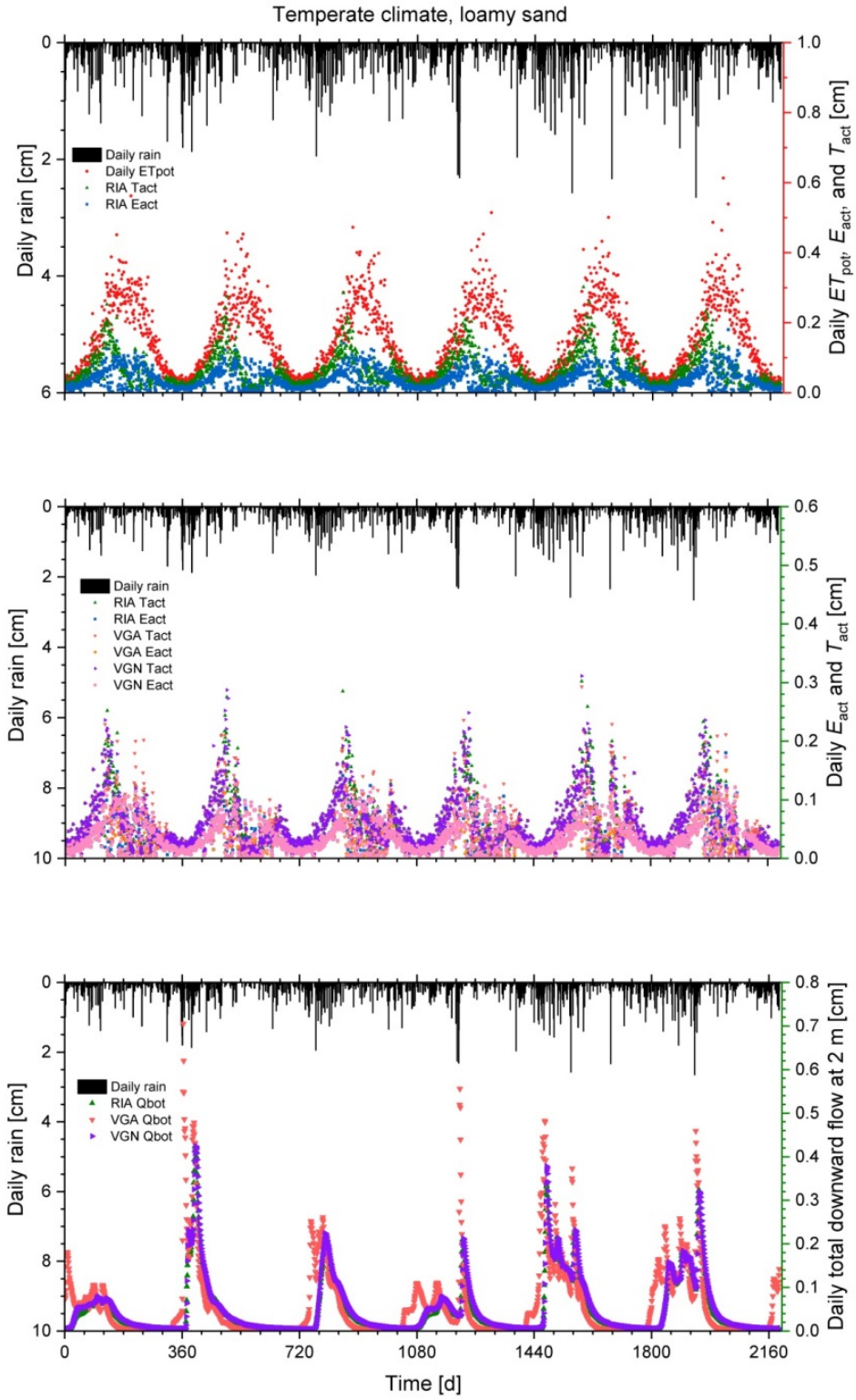

Figure S9. Like Fig. S3, but for a temperate climate.

References

Brown, R. N., Percivalle, C., Narkiewicz, S., and DeCuollo, S.: Relative rooting depths of native grasses and amenity grasses with potential for use on roadsides in New England, HortSience 45, 393–400, 2010.

Davies, J. A.: A note on the relationship between net radiation and solar radiation, Quarterly Journal of the Royal Meteorological Society, 93, 109–115, 1967.

de Rooij, G. H.: A simple weather generator for applications with limited data availability: TEmpotRain 1.0 for rainfall, temperatures, extraterrestrial radiation, and potential evapotranspiration, Geosci. Model Dev. Discuss., doi: 10.5194/gmd-2018-97, 2018.

Droogers, P., and Allen, R. G.: 2002. Estimating reference evapotranspiration under inaccurate data conditions, Irrigation and Drainage Systems, 16, 33–45, 2002.

Evett, S. R.: Energy and water balances at soil–plant–atmosphere interfaces, in: Handbook of soil science, edited by Sumner, M. E. editor, CRC Press, Boca Raton, Fla., U.S.A., A129 – A182, 2000.

Grant, I. F., Prata, A. J., and Cechet, R. P.: The impact of diurnal variation of albedo on the remote sensing of the daily mean albedo of grassland, J. Appl. Meteorology, 39, 231–244, doi: 10.1175/1520-0450(2000)039<0231:TIOTDV>2.0.CO;2, 2000.

Pham, M. T., Vanhaute, W. J., Vanderberghe, S., De Baets, B, and Verhoest, N. E. C.: An assessment of the ability of Bartlett–Lewis type of rainfall models to reproduce drought statistics, Hydrol. Earth Syst. Sci., 17, 5167–5183, doi:10.5194/hess-17-5167-2013, 2013.

Šimůnek, J., Šejna, M., Sait., H., Sakai, M., and van Genuchten, M. Th.: The HYDRUS–1D software package for simulating the one–dimensional movement of water, heat, and multiple solutes in variably–saturated media, Version 4.17, Dept. Env. Sci., Univ. Calif., Riverside, CA, U.S.A., 2013.